CrossMark

Propagation of Solar Energetic Particles During Multiple Coronal Mass Ejection Events

Silja Pohjolainen[1] · **Firas Al-Hamadani**[2,3] ·
Eino Valtonen[2]

Abstract We study solar energetic particle (SEP) events during multiple solar eruptions. The analysed sequences, on 24 – 26 November 2000, 9 – 13 April 2001, and 22 – 25 August 2005, consisted of halo-type coronal mass ejections (CMEs) that originated from the same active region and were associated with intense flares, EUV waves, and interplanetary (IP) radio type II and type III bursts. The first two solar events in each of these sequences showed SEP enhancements near Earth, but the third in the row did not. We observed that in these latter events the type III radio bursts were stopped at much higher frequencies than in the earlier events, indicating that the bursts did not reach the typical plasma density levels near Earth. To explain the missing third SEP event in each sequence, we suggest that the earlier-launched CMEs and the CME-driven shocks either reduced the seed particle population and thus led to inefficient particle acceleration, or that the earlier-launched CMEs and shocks changed the propagation paths or prevented the propagation of both the electron beams and SEPs, so that they were not detected near Earth even when the shock arrivals were recorded.

✉ S. Pohjolainen
silpoh@utu.fi

F. Al-Hamadani
fimubaa@utu.fi

E. Valtonen
eino.valtonen@utu.fi

[1] Tuorla Observatory, University of Turku, Piikkiö, Finland

[2] Department of Physics and Astronomy, University of Turku, Turku, Finland

[3] Department of Physics, University of Basrah, Basrah, Iraq

🍂 Springer

1. Introduction

Solar energetic particles (SEPs) are believed to be first accelerated in the lift-off phase of coronal mass ejections (CMEs). The SEP acceleration itself could be due to flaring processes, acceleration in coronal and/or interplanetary shocks, or it could be a combination of all (Trottet *et al.*, 2015). Diffusive shock acceleration near the Sun of a population of seed particles with suprathermal energies has been suggested as one alternative (Tylka and Lee, 2006). Recently, Kahler and Vourlidas (2014b) studied whether the background solar wind speed could affect the SEP event timescales, but no differences were found.

Radio emission can be used as a probe to identify particle acceleration in the solar corona and interplanetary (IP) space. Solar type III radio bursts are observed when accelerated electrons travel outward in the solar corona and propagate along open magnetic field lines. They excite plasma oscillations at the local plasma frequency, which are then converted into radio waves at the fundamental and harmonic plasma frequencies (Dulk, 2000). The fast frequency-drifting radio emission of the type III bursts is due to fast electron beams, typically originating from solar flares. Solar type II radio bursts show a much slower frequency drift and a wider emission band than type III bursts. The emission mechanism for type II bursts is basically the same as for type IIIs, with the difference that the accelerated electrons are believed to originate from propagating shocks. The emission features reflect the speed of the shock and the short propagation paths of shock-accelerated electrons, see review by, *e.g.*, Gopalswamy (2000). In the interplanetary space these shocks are usually CME driven.

Dependences of SEP enhancements in multiple CME events have been investigated in several studies (Gopalswamy *et al.*, 2004; Kahler and Vourlidas, 2005; Ding *et al.*, 2013; Kahler and Vourlidas, 2014a). Al-Sawad *et al.* (2009) and Kocharov *et al.* (2009) presented cases where two CMEs were launched close in time and both eruptions were associated with SEP enhancements. In both of these analyses it was suggested that the first shock weakens and becomes gradually transparent for the protons produced by the second eruption, behind the first CME.

In this article we analyse triple events where the first two CMEs are associated with SEP enhancements, but at the time of the third CME no SEP enhancement is observed. We use solar radio data and *in-situ* magnetic field measurements to investigate how particle beams and shock fronts propagate during these time periods, to determine whether the particle propagation conditions or acceleration processes change in the course of the successive events.

2. Data Analysis

The aim of this study is to investigate how energetic particles can propagate during multiple solar eruptions. Our basic selection criterion for the analysed events was that there had to be at least three consecutive CMEs that originated from the same active region within three-four days. Each of the CMEs had to be associated with an IP radio type II burst, since this type of burst can be considered as a sign of a propagating shock wave that is capable of accelerating particles. The *Wind/Plasma and Radio Waves* (WAVES) list of type II bursts and CMEs at http://cdaw.gsfc.nasa.gov/CME_list/radio/waves_type2.html was used to find event sequences that matched our requirements. The preliminary candidate list that consisted of 17 sequences of consecutive events is presented in Table 5 (Appendix).

For the analysis, the CMEs had to be separable from each other so that their associated features could be investigated. In some cases the CMEs occurred so close in time to each

other that their individual properties could not be separated (these could be called early CME interaction events). Energetic particles had to be observed with the first two CMEs, and this requirement removed from our list those events that were not well-connected to the field lines near L1, where the *Energetic and Relativistic Nuclei and Electron* (ERNE: Torsti *et al.*, 1995) instrument onboard the *Solar and Heliospheric Observatory* (SOHO) is located. Data gaps in the *in-situ* particle data also made the analysis impossible for some of the events. Eventually, three triple events were selected for closer inspection.

The SOHO/*Large Angle and Spectrometric Coronagraph* (LASCO) CME Catalog at http://cdaw.gsfc.nasa.gov/ was used to find the CME characteristics (width, speed, height–time evolution). The data for the associated IP radio type II events were taken from the *Wind*/WAVES (Bougeret *et al.*, 1995) catalogue at http://lep694.gsfc.nasa.gov/waves/data_products.html, prepared by Michael L. Kaiser. Flares and flare locations were checked from the NOAA National Geophysical Data Center (NGDC) flare listings at http://www.ngdc.noaa.gov/stp/spaceweather.html. X-ray data from the *Geostationary Operational Environmental Satellite* (GOES) were plotted using *Solarsoft* to check the listings and to identify multiple flare events. The SOHO/*Extreme-Ultraviolet Imaging Telescope* (EIT: Delaboudinière *et al.*, 1995) images were searched to find EUV waves and dimmings.

The SOHO/ERNE proton data were then investigated using the website at http://www.srl.utu.fi/erne_data/main_english.html to find the associated SEP events. As supportive observations we used electron data from *Advanced Composition Explorer/Electron, Proton and Alpha Monitor* (ACE/EPAM: Gold *et al.*, 1998) and SOHO/*Electron Proton Helium Instrument* (EPHIN: Müller-Mellin *et al.*, 1995) from the SEPServer (Vainio *et al.*, 2013) at http://server.sepserver.eu/index.php. The ACE/*Magnetometer instrument* (MAG: Smith *et al.*, 1998) magnetic field measurements available at http://www.srl.caltech.edu/ACE/ASC/level2/lvl2DATA_MAG.html were used for assessing the local magnetic field conditions at the time of the SEP events.

To verify the shock arrival near Earth, we checked the ACE, *Wind*, and SOHO/*Charge, Element, and Isotope Analysis System* (CELIAS) shock lists at http://www.cfa.harvard.edu/shocks/ and at http://umtof.umd.edu/pm/FIGS.HTML. Interplanetary CME (ICME) arrival times were verified from http://www.ssg.sr.unh.edu/mag/ace/ACElists/ICMEtable.html.

To compare the CME heights with shock heights, we calculated the radio source heights for the observed IP type II bursts. The observed radio frequency [f] in Hz depends on the local electron density [n_e] in cm^{-3} by $f = 9000\sqrt{n_e}$. The methods of determining type II burst heights using atmospheric density models are described in, *e.g.*, Pohjolainen *et al.* (2007). The hybrid electron density model of Vršnak, Magdalenić, and Zlobec (2004) was selected for the calculations, mainly because it merges the high-density low-corona models into the low-density IP models without breaks or discrepancies.

2.1. Events on 24 – 26 November 2000

On 24 November 2000, three GOES X-class flares were observed to originate from the same active region, NOAA 9236. The flares were associated with fast halo-type CMEs, and their approximate initial speeds are listed in Table 1. Two C-class flares (C4.2 and C2.4) were reported between the X2.0 and X2.3 flares from the same active region. Between the X2.3 and X1.8 events, no flares were reported from this active region. All three flare–CME events were associated with an IP radio type II burst, as seen in the *Wind*/WAVES dynamic spectrum in Figure 1. The type II emission lanes are enhanced with white dashed lines.

The first IP type II burst was rather complex in its beginning, but it was very intense, with a clear narrow-band emission lane at frequencies below 1 MHz. The calculated type II

Table 1 Solar events observed during 24 – 26 November 2000.

Date	Flare start UT	Flare site	Flare class GOES	CME speed km s^{-1}	Shock arrival and speed[a] ACE km s^{-1}	Shock arrival and speed[a] *Wind*[c] km s^{-1}
2000 Nov. 24	04:55	N20W06	X2.0	1300	Nov 26, 05:00/462	05:32/520
2000 Nov. 24	14:51	N22W08	X2.3	1240	Nov 26, 11:24/632	11:43/666
2000 Nov. 24	21:43	N21W14	X1.8	1000[b]		

[a]Shock velocity is given after the slash.

[b]Estimated speed using the last two CME height observations is 1240 km s^{-1}.

[c]*Wind* near Earth, distance to ACE $\sim$ 950 000 km.

source heights fit well with the CME heights, as shown by the height–time plot in Figure 1 (bottom panel, type II heights are indicated with red filled circles). The second type II burst was comprised of narrow-band short-duration bursts, with a separate, more diffuse emission lane at lower frequencies. We used this lower frequency lane for the height calculations, and the obtained heights again agree well with the corresponding CME heights. The third type II burst was visible only down to 3 MHz, and the calculated type II heights match those of the CME in its early phase.

All three flare–CME events were also associated with radio type III bursts. The first two continued down to the plasma density level near Earth, to about 30 kHz, but the third ended at about 200 kHz. This plasma frequency corresponds to an electron density of 494 cm^{-3}, which in standard atmospheric density would be at a distance of about 30 R$_\odot$ from the Sun centre. At the time of the type III cut-off start, the leading front of the first CME was estimated to have a height of about 100 R$_\odot$ and the second CME front a height of about 40 R$_\odot$. The radio dynamic spectrum shows little difference between the frequency of the second type II burst and the type III end-frequency near the time of the cut-off start, suggesting that the type III cut-off occurred approximately at the height where the shock front of the second CME is located.

The strong type III burst after the third event, in the early hours of 25 November, originated from a flare at N07E50, with an eastward-directed CME. Hence it had a completely different magnetic connectivity to Earth than the three earlier events. During most part of the day on 25 November, the type III bursts associated with flares in AR NOAA 9236 had similar shorter propagation paths, and their emission ended near 200 kHz.

Before the first X-class flare at 04:55 UT on 24 November, several radio type III bursts occurred that originated from the same active region NOAA 9236 and were observed to have a cut-off at the second harmonic of the local plasma frequency ($2f_p$). Two local plasma frequency emission lanes ($\sim$ 20 and $\sim$ 40 kHz) were clearly visible in the dynamic spectra during several days before the type III burst activity on 23 November. However, the strong type III burst emission associated with the first X-class flare at 04:55 UT was able to reach the fundamental plasma frequency level, and by that time the second harmonic lane had also disappeared from the spectrum.

The ERNE *in-situ* observations of energetic protons show two enhancements, the first associated with the start of the first CME-type II event and the second with the start of the second CME-type II event. At the time of the start of the third CME-type II event, the SEP flux was decreasing at all energies (Figure 1, top panel).
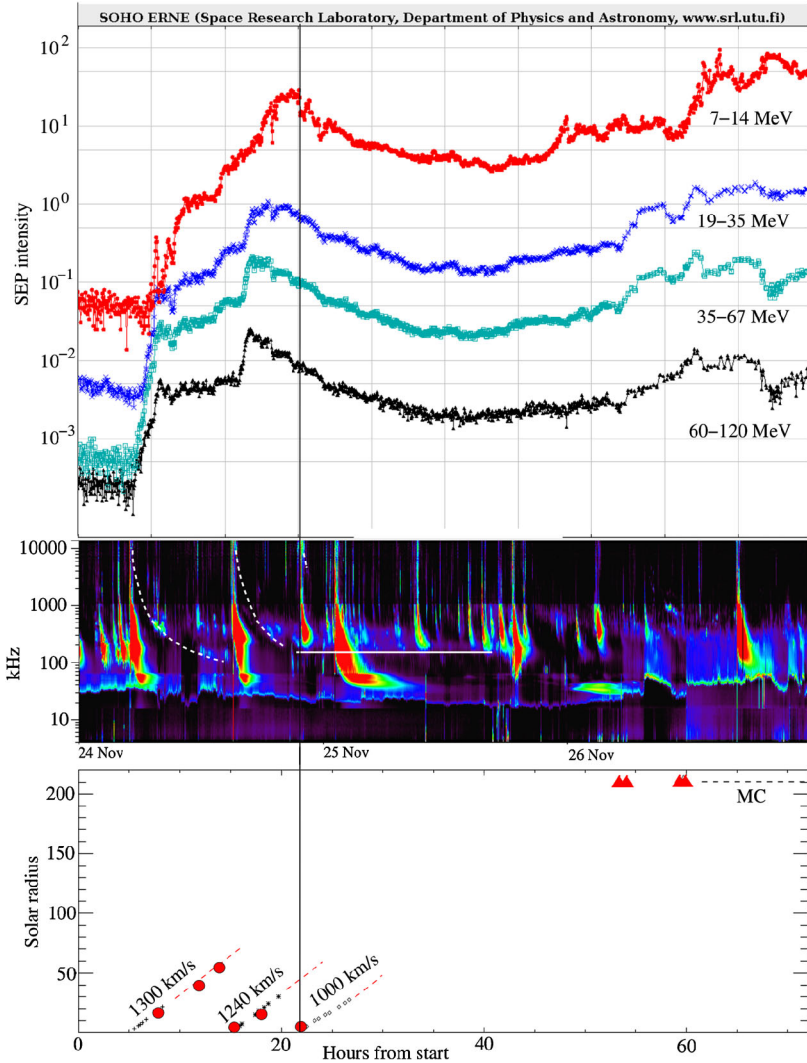
Figure 1 Solar events on 24–26 November 2000: Solar energetic proton intensities observed *in-situ* by SOHO/ERNE, in $(cm^2\,s\,sr\,MeV)^{-1}$ (top panel, energy range 7–120 MeV). The *Wind*/WAVES radio dynamic spectrum (middle panel, frequency range 14 MHz–4 kHz) shows the associated IP type II bursts (the lanes are enhanced with white dashed lines) and the period of type III burst cut-offs (white horizontal line). The type III burst in the early hours of 25 November that shows no cut-off originated from an active region located near the East limb. The height–time plot (bottom panel) shows the associated CMEs and their estimated initial velocities, the calculated type II heights (red circles), and the times of shock arrival near L1 and Earth (red triangles). The black vertical line marks the time after which a SEP enhancement would have been expected to appear. The black dashed line marks the MC-like structure reported by Wang, Wang, and Ye (2002).

At least two shocks were observed to arrive near Earth, recorded by ACE (near L1) and *Wind* (near Earth) on 26 November. They are listed in Table 1 with the shock arrival speeds. In Figure 1 the shock arrival times are indicated with red triangles in the height–time plot in the bottom panel. The SOHO/CELIAS list also contains two possible shocks on

Table 2 Solar events observed during 9 – 13 April 2001

Date	Flare start UT	Flare site	Flare class GOES	CME speed km s^{-1}	Shock arrival and speed[a] ACE km s^{-1}	Shock arrival and speed[a] *Wind*[b] km s^{-1}
2001 Apr. 9	15:20	S21W04	M7.9	1200	Apr 11, 13:14/613	14:09/673
2001 Apr. 10	05:06	S23W09	X2.3	2400	Apr 11, 15:28/731	16:18/828
						18:18/830
2001 Apr. 11	12:56	S22W27	M2.3	1100	Apr 13, 07:06/914	

[a]Shock velocity is given after the slash.

[b]*Wind* near Earth, distance to ACE $\sim 1\,400\,000$ km.

26 November. The arrival time of the first (07:15 UT) is two hours later than the ACE and *Wind* shocks, but the second (11:26 UT) fits the other observations well. The travel times and CME speeds suggest that these shocks could be associated with the first two CMEs and, with some caution, also with the third CME. For example Wang, Wang, and Ye (2002) have suggested that the second shock could have been produced by several merging shocks.

Wang, Wang, and Ye (2002) reported an IP magnetic cloud (MC) -like structure observed by the *Wind* satellite starting at about 13:00 UT on 26 November. They proposed it to be the result of at least four halo CMEs, of which the first three are the homologous CMEs analysed here. Later on, there are two listed ICME passages on 27 and 28 November. Cane and Richardson (2003) have reported them as multiple CME events, the 27 November ICME as the result of the CMEs on 24 November and the 28 November ICME as the result of several CMEs that occurred during 25 – 26 November.

2.2. Events on 9 – 13 April 2001

In April 2001 three consecutive CME and IP type II burst-associated flares originated from the same active region, NOAA 9415, observed on 9, 10, and 11 April. The flares were GOES class M7.9, X2.3, and M2.3, respectively. The flares and the high-speed halo-type CMEs are listed in Table 2. Between the M7.9 and X2.3 flares, one C2.1 flare was reported from active region NOAA 9415. Between the X2.3 and M2.3 flares there was one C2.7 flare. The associated IP type II bursts are visible in the *Wind*/WAVES dynamic spectrum in Figure 2 (enhanced with white dashed lines).

The radio dynamic spectrum shows a short-duration IP type II burst at 12 – 7 MHz on 9 April, but intermittent emission was also observed at lower frequencies. We measured the type II burst heights using this lower, less intense emission lane. The type II source heights agree well with the heights of the associated CME (Figure 2, bottom panel). The next IP type II burst on 10 April had a very wide and diffuse emission band, and the height was calculated using the emission lane centre. Similar to some of the wide-band events reported in Pohjolainen, Allawi, and Valtonen (2013), the velocity of the type II burst source decreased rapidly and the burst showed a different height–time evolution than the associated CME. The third IP type II burst on 11 April had a narrow band and was visible for less than two hours from the beginning of the flare–CME event. The type II heights matched those of the CME in its initial phase.
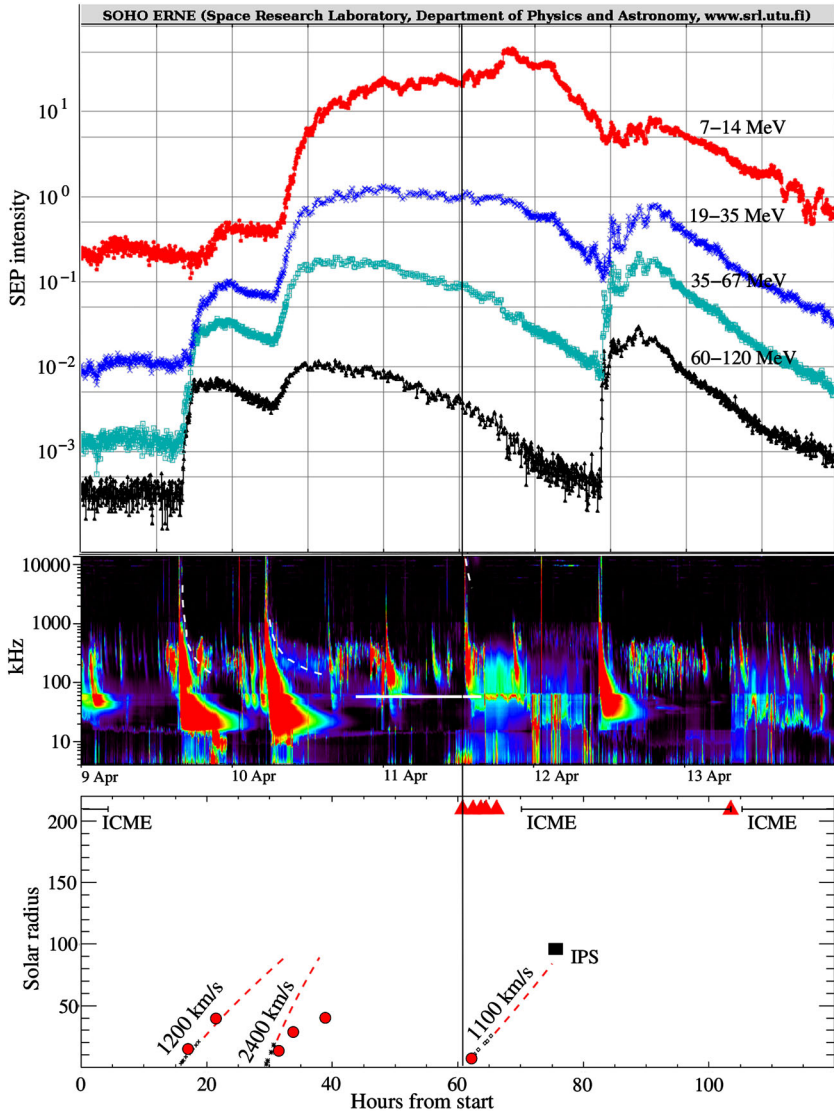
Figure 2 Solar events on 9 – 13 April 2001, panels, symbols, and units are the same as in Figure 1. The black box marks the estimated CME height from IPS measurements reported by Iju, Tokumaru, and Fujiki (2013).

All three flare–CME events were also associated with radio type III bursts. The first two type IIIs continued down to the plasma level near Earth, to about 30 kHz, but the third ended near 60 kHz. In standard atmospheric density this would mean a distance of about 90 $R_{\odot}$ from the Sun centre. At the time of the cut-off, the leading edges of the earlier two CMEs were both estimated to be at a height of about 150 $R_{\odot}$. The third type III event was also associated with prolonged enhanced radio emission observed around 50 – 100 kHz. This period coincides with the detection of several shock arrivals near Earth (indicated by red

triangles in Figure 2), so it could be associated with local shocks caused by the earlier two CMEs that had merged during their propagation.

For the third event there are interplanetary scintillation (IPS) measurements of the CME height (Iju, Tokumaru, and Fujiki, 2013). The CME was estimated to be at a height of 95 R$_{\odot}$ at 03:34 UT on 12 April. This position is in line with the CME-type II heights from the start to the arrival of the shock near Earth on 13 April 07:06 UT (Figure 2, bottom panel).

The *in-situ* observations of energetic particles show two enhancements, the first associated with the first CME-type II start and the second with the second CME-type II start. At the time of the third CME-type II start the SEP flux curve was decreasing at higher energies. We note that the next flare–CME event from active region NOAA 9415 was on 12 April and was again associated with a SEP enhancement, but this time it was more pronounced in the higher energies. This flare–CME event was associated with a metric type II burst, but no IP type II emission was observed. Between the 12 April flare and the preceding, analysed M2.3 flare on 11 April three other flares (C7.7, B7.2, and M1.3) occurred in the same active region. As the 12 April SEP event was observed inside the earlier-launched ICMEs, there could have been a direct connection to the active region.

Several shocks were observed to arrive near Earth, recorded by ACE (near L1) and *Wind* (near Earth) on 11 and 13 April (Table 2 and Figure 2, bottom panel). SOHO/CELIAS also observed the first two shock arrivals on 11 April (13:02 and 15:18 UT), as well the shock arrival on 13 April (07:05 UT). The shocks on 11 April seem to be associated with the first two CME-type II events, which probably had merged during propagation. The shock on 13 April could be connected with the third CME-type II event, as the IPS observation of the CME is located in between the start of the CME and the shock arrival. However, we cannot rule out the possibility that the 13 April shock was associated with the decelerating, wide-band type II burst observed on 10 April.

Several ICME passages have been reported for these dates (Cane and Richardson, 2003). The updated list of Near-Earth Interplanetary Coronal Mass Ejections, compiled by Ian Richardson and Hilary Cane, online at http://www.srl.caltech.edu/ACE/ASC/DATA/level3/icmetable2.htm, reports an earlier ICME passage that started on 8 April and continued until 04:00 UT on 9 April. The next passage started at 22:00 UT on 11 April and ended at 07:00 UT on 13 April. The following ICME passage started two hours later on the same day and ended on 14 April.

2.3. Events on 22 – 25 August 2005

Three consecutive GOES M-class flares were observed to originate from the same active region NOAA 10798 on 22 – 23 August 2005. The flares were associated with fast halo-type CMEs, and their approximate initial speeds are listed in Table 3. Between the M2.6 and M5.6 flares two B-class flares (B5.2 and B5.3) were reported from the active region. Between the second and third flare in Table 3, no flares were reported from this active region. All three flare–CME events were also associated with an IP type II burst, see the *Wind*/WAVES dynamic spectrum in Figure 3.

The first IP type II burst on 22 August had a strong, narrow emission lane that could be followed from 2 MHz down to 400 kHz. The calculated type II burst source heights agree well with the CME heights, see Figure 3, bottom panel. The next type II burst on the same day was more chaotic, with patches of emission superposed on weaker emission. We used the diffuse emission lane centre for the height calculations, and the match with the CME heights is again good. We note that from 01:00 to 06:00 UT on 23 August there are enhanced radio emission features at 80 – 50 kHz (they appear as blob-like structures

Table 3 Solar events observed during 22 – 25 August 2005

Date	Flare start UT	Flare site	Flare class GOES	CME speed km s^{-1}	Shock arrival and speed[a] ACE km s^{-1}	Shock arrival and speed[a] Wind[d] km s^{-1}
2005 Aug. 22	00:44	S11W54	M2.6	1190		
2005 Aug. 22	16:46	S13W65	M5.6	2400	Aug 24, 05:45/581	05:35/591
					Aug 24, 08:20/795	08:24/525
2005 Aug. 23	14:19	S14W75[b]	M2.7	1900	Aug 25, 13:00[c]	

[a]Shock velocity is given after the slash.

[b]Estimated flare location on the disk S14W75–80, flare loop top above the limb.

[c]See Papaioannou *et al.* (2009).

[d]*Wind* near ACE at L1.

in the radio dynamic spectrum, indicated with a white arrow in Figure 3), which could be signatures of CME interaction. The corresponding distance from the Sun centre is about $65 – 100$ R$_\odot$, which is a realistic height when looking at the height–time data of the first two CMEs and the related type II shocks. The third type II burst on 23 August showed very clear and narrow emission bands both at the fundamental and harmonic plasma frequencies. The lanes continued down to about 300 kHz before they became mixed with other emission features. The calculated type II heights, however, are considerably lower than the estimated CME heights after the event start, similar to the wide-band type II shock on 10 April 2001, described in Section 2.2.

The three flare–CME events were also associated with radio type III bursts. The first two type IIIs continued down to the plasma density level near Earth, to about 30 kHz, but the third ended near $50 – 80$ kHz (corresponding to the same distance as for the earlier possible CME interaction signatures). The end frequency of the third type III burst is not easily determined as there is also additional enhanced emission present (non-drifting and slowly drifting). The estimates of the leading front heights of the earlier two CMEs at the time of the type III cut-off start give heights of about $180 – 160$ R$_\odot$, respectively, but as the first CME was decelerating and the second CME was accelerating, they could have already merged, as suggested by the blob-like emission structures at $80 – 50$ kHz observed some hours earlier.

The *in-situ* observations of energetic particles show two enhancements, the first associated with the first CME-type II start and the second with the second CME-type II start (Figure 3, top panel). At the time of the third CME-type II start, the SEP flux was decreasing in all energy ranges.

The first two close-in-time shock arrivals were recorded by ACE and *Wind* (both near L1) on 24 August (Table 3 and Figure 3, bottom panel). They seem to be associated with the first two CME-type II events that were launched on 22 August. SOHO/CELIAS lists only one shock (05:34 UT) that is near the times of the first shock reported by ACE and *Wind*. For the third CME-type II event that was launched on 23 August, Papaioannou *et al.* (2009) reported a disturbance observed by ACE on 25 August at 13:00 UT. A minor geomagnetic storm was observed to follow at $15:00 – 18:00$ UT.

The Richardson and Cane list of Near-Earth Interplanetary Coronal Mass Ejections contains two ICME passages for 24 August. The first started at 00:00 UT and ended at 11:00
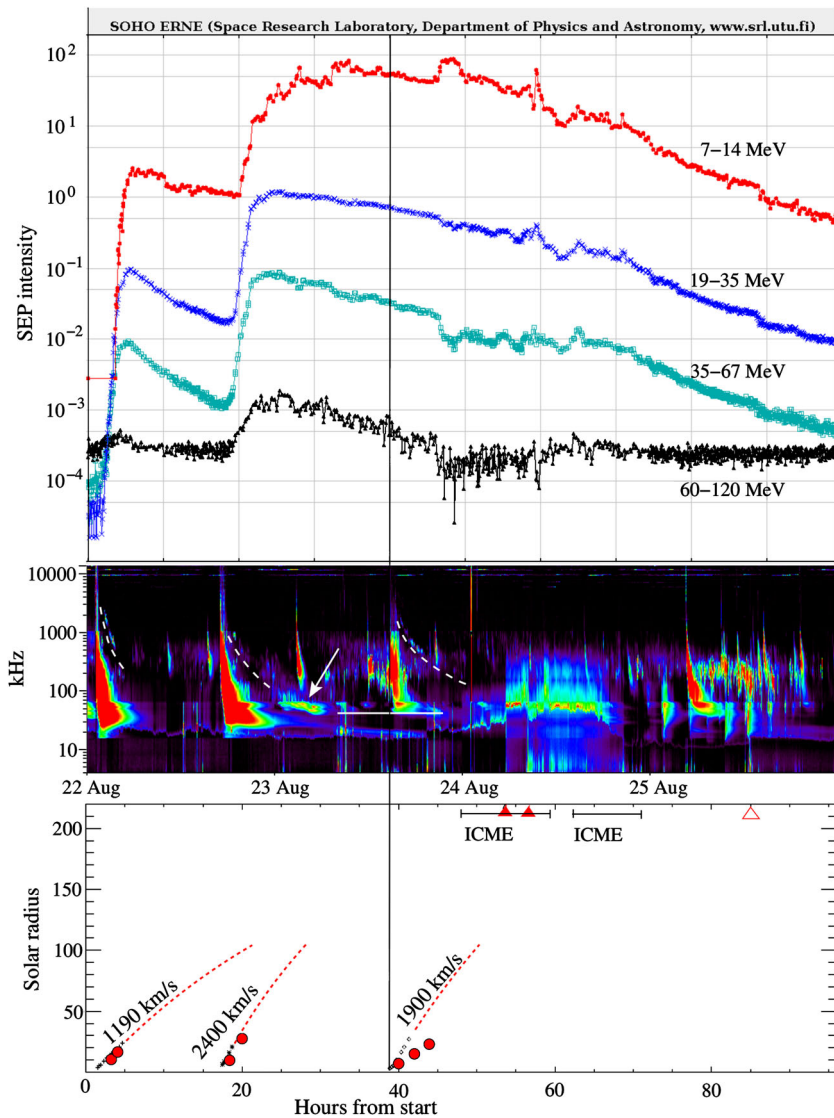
Figure 3 Solar events on 22 – 25 August 2005, panels, symbols, and units are the same as in Figure 1. The white arrow in the radio dynamic spectrum points to the blob-like structures discussed in the text. The red unfilled triangle indicates the time of a disturbance reported by Papaioannou *et al.* (2009).

UT, the second started at 14:00 UT and ended at 23:00 UT. A geomagnetic storm was also reported at 11:00 UT (Uwamahoro, McKinnell, and Habarulema, 2012).

2.4. SEP Characteristics and Interplanetary Conditions

The results from the SEP data analysis are summarized in Table 4. The table also gives the flare start times and the CME heights at the estimated times of first SEP injection.

Table 4 SEP characteristics and other observed features

Date	Flare start (UT)	SEP injection (UT)	Time from flare start (hours)	CME height ($R_\odot$)	Path length (AU)	EUV wave (UT)
2000 Nov. 24	04:55	$05:21 \pm 14$	0.43	~ 2.5	2.09 ± 0.19	05:12
2000 Nov. 24	14:51	15:27	0.60	~ 3.0	1.5 (highest energy)	15:12
2000 Nov. 24	21:43	–				22:00
2001 Apr. 9	15:20	16:01	0.68	~ 4.0	1.2 (fixed length)	15:36
2001 Apr. 10	05:06	$06:48 \pm 11$	1.70	~ 19.0	1.38 ± 0.15	05:24
2001 Apr. 11	12:56	–				13:13
2005 Aug. 22	00:44	$01:29 \pm 9$	0.75	~ 4.0	1.62 ± 0.12	01:13
2005 Aug. 22	16:46	17:30	0.70	~ 6.0	1.2 (fixed length)	17:12
		$18:22 \pm 9$	1.60	~ 16.0	2.06 ± 0.09	
2005 Aug. 23	14:19	–				14:48

2.4.1. 24 November 2000

The ERNE *in-situ* observations of solar protons at energies $1-130$ MeV showed two enhancements on 24 November 2000 (Figure 1). These events occurred on the tail of the very large and long-duration event on 8 November. At the time of the first event onset, the background was approximately at the quiet-time level only at the highest energies (> 50 MeV). The onset of the event was, however, clearly visible at all energies up to 100 MeV. A velocity dispersion analysis (VDA) indicated a release time of protons at the Sun at 05:21 UT $\pm$ 14 minutes with an apparent path length of 2.09 ± 0.19 AU (Vainio *et al.*, 2013). Thus, the release time of the particles is well associated with the first flare (04:55 UT) and the CME, which at the time of the estimated particle release time was at a height of $2-3$ $R_\odot$.

The onset of the second event was strongly masked by the first event, but was well visible at the highest energies to beyond 100 MeV. At energies below ~ 20 MeV it was hardly distinguishable from the still rising intensities related to the first event roughly 10 hours before. The VDA of this event, by using only the highest energy channels ($17-130$ MeV), give a release time at 15:27 UT with an apparent path length of 1.5 AU. The release time agrees reasonably well with the flare timing (14:51 UT), with a CME height of about 3 $R_\odot$ at the time of the particle release.

At the time when the third flare was observed (21:43 UT) and when the associated CME was at a height of about 3 $R_\odot$ (~ 22 UT), no sign of a proton enhancement was observed at any energy channel. Later on, on 25 November at about 15:00 UT, the intensities started rising slowly, probably related to the fast eastern halo CME at 01:32 UT on 25 November. On 26 November small SEP enhancements were visible at lower energies, which may be related to the shock arrivals indicated in Figure 1.

We also inspected the electron data from ACE/EPAM and SOHO/EPHIN. We used ACE/EPAM deflected electron channels at $0.103-0.175$ MeV and $0.175-0.315$ MeV and SOHO/EPHIN electron channels at $0.25-0.7$ MeV and $0.67-3$ MeV. Electrons associated with the two first flare–CME events were clearly visible, but no enhancement was observed at the time of the third event. We also used the $0.175-0.315$ MeV and $0.67-3$ MeV channels of ACE/EPAM and SOHO/EPHIN, respectively, to determine the release times of electrons by assuming a nominal path length of 1.2 AU for the particles. The release times obtained

were 05:32 UT (EPAM) and 05:12 UT (EPHIN) for the first and 15:32 UT (EPAM) and 15:33 UT (EPHIN) for the second event. These are consistent with the proton release times (Table 4).

To assess effects of interplanetary conditions on propagation of particles possibly accelerated during the third flare–CME event, we investigated ACE/MAG magnetic field data. We studied both the large-scale sector structure of the interplanetary magnetic field and possible smaller scale flux-rope structures at the time of the three events that could have changed the propagation paths of protons from the third event so that they would remain undetected at Earth. We used measurements of magnetic field components in Geocentric Solar Ecliptic (GSE) coordinates, with time resolution ranging from 1 hour to 16 seconds, as appropriate for the studied structures. A polarity change of the interplanetary magnetic field (IMF), from away to towards the Sun, occurred on 23 November just before the first event of the November 2000 sequence, and the polarity reversed again on 1 December. During the early hours of 24 November, there were periods of strong fluctuations in the magnetic field direction and a slow rotation of the field between about 07:15 UT and 09:30 UT, possibly related to a flux-rope structure. At the time of all three flare–CME and SEP events of 24 November, the magnetic field had the same polarity with approximately the same direction close to the nominal Parker spiral. However, these *in-situ* measurements do not reveal the configuration of the IMF between the Sun and Earth at the time of particle propagation through the IP space. Obviously, the shock structure related to the first CME did not prevent protons of the second event from reaching the Earth. However, the first and second shocks together might have blocked the way of the protons associated with the third flare–CME event. These shock structures and a magnetic cloud were detected at Earth on 26 November (see Figure 1).

2.4.2. 9 – 11 April 2001

The *in-situ* observations of energetic particles showed two enhancements on 9 – 10 April 2001 (Figure 2). These enhancements were preceded by a series of three major SEP events starting at the end of March, and the background was high at all energies < 50 MeV. Because of the background, the first enhancement was not observable below 5 MeV, but at higher energies it was visible up to ~ 90 MeV. The initial VDA did not give a reasonable result (Vainio *et al.*, 2013). In this event, the VDA gives an unreasonably long path length (4 – 7 AU, depending on which energy channels are used), indicating that the assumptions behind the VDA are not valid. By inspecting the intensity–time profiles, the earliest onset time of all energy channels was found to be at 16:18 UT at 90.5 MeV. By assuming a path length of 1.2 AU, this would result in a release time at 15:53 UT at the Sun (plus 8 minutes to be comparable with electromagnetic observations). This proton release time was consistent with the derived electron release times of ACE/EPAM (16:02 UT) and SOHO/EPHIN (16:00 UT). This also agrees reasonably well with the flare start time (15:20 UT) and the CME observation at the height of $\sim 4\,\mathrm{R}_\odot$.

During the second SEP enhancement, the intensities below 10 MeV rose two orders of magnitude above the level of the first one, and at ~ 35 MeV they were still an order of magnitude above the previous one. At 90 MeV this second event was no longer very pronounced, but still rose to the peak level ($\sim 5 \times 10^{-3}$ cm^{-2} s^{-1} sr^{-1} MeV^{-1}) of the first already decaying event at this energy. For this second event, the VDA gives a release time at 06:48 UT $\pm$ 11 minutes and an apparent path length of 1.38 $\pm$ 0.15 AU. Because of the high background and slowly rising profiles it is difficult, however, to observe the first-arriving particles, thus increasing the uncertainty of the VDA results. The obtained SEP release time is quite late compared to the flare time (05:06 UT), and at that time the second

CME was already at the height of $\sim 19 \, R_\odot$. The obtained electron release times associated with the second flare–CME event were 05:58 UT (EPAM) and 06:26 UT (EPHIN), which are somewhat earlier than the derived proton release time. No other major flares or fast CMEs were observed during the early hours of 10 April. Therefore, although the VDA results would be unreliable, it seems reasonable to assume that the cause of the observed particle enhancement at 06:40-06:50 UT is the flare–CME event of 10 April at 05:06/05:30 UT.

As in November 2000, no particle enhancement was observed that could have been associated with the third flare–CME-type II burst events. On 11 April from 13:00 to 14:00 UT, after the flare and while the CME was still below the height of about 6 $R_\odot$, the proton intensities above ~ 25 MeV were slowly decaying. At the lowest energies the intensities were slowly rising, probably due to the approaching shocks (Table 2), peaking at $\sim 19:20$ UT after the last reported shock in the *Wind* observations. A small drop in intensities was also observed at middle energies, coincident with the arrival of the ICME (Figure 2). A slow enhancement in ACE/EPAM and SOHO/EPHIN electron intensities, most probably associated with the shock arrival, was also observed to start at about 13:00 UT.

We again studied the magnetic field data to find a possible reason for not detecting protons associated with the third flare–CME event, due to interplanetary conditions. During all three events SOHO was located in the same polarity sector with a field direction close to the nominal Parker spiral. No flux-rope structures were observed. The magnetic field strength remained relatively stable during the events, although immediately after the third flare–CME event there was a sudden increase particularly in the x-component of the magnetic field, related to the shock arriving at SOHO. This shock structure might have changed the path of particles, possibly associated with the third flare–CME event, diverting them away from SOHO.

2.4.3. 22 – 23 August 2005

Two proton enhancements were observed by ERNE on 22 August 2005. The first occurred at quiet-time background. The intensities rose rapidly by approximately two orders of magnitude, up to 50 MeV energies (Figure 3). At 72 MeV this event was no longer well visible. For this event, the VDA gives a release time at 01:29 UT $\pm$ 9 minutes, with an apparent path length of 1.62 $\pm$ 0.12 AU. The derived electron release times are slightly earlier: 01:09 UT (0.175 – 0.315 MeV, EPAM) and 01:04 UT (0.67 – 3 MeV, EPHIN). The proton release time, however, matches the flare start time (00:44 UT) reasonably well. The associated CME was then at the height of $\sim 4 \, R_\odot$.

The separation of the two particle events was only about 15 hours, which means that the second event occurred on the tail of the first. Excluding the lowest energies (< 3 MeV), this event was clearly distinguishable, however, with the intensities exceeding the peak intensities of the first event by at least one order of magnitude at all energies up to 72 MeV, and was still visible at 90 MeV. The release time was estimated to be 18:22 UT $\pm$ 9 minutes, with an apparent path length of 2.06 $\pm$ 0.09 AU. This is again relatively late compared with the flare start time (16:46 UT), while the associated CME was at a height of $\sim 16 \, R_\odot$. An estimate based on the earliest observed onset at 57.4 MeV provides the release time at $\sim 17:30$ UT using a 1.2 AU path length, at which time the associated CME was at a height of $\sim 6 \, R_\odot$. It is therefore reasonable to assume that this SEP event was associated with the M5.7 flare at 16:46 UT and the CME that was first observed at 17:30 UT. The derived electron release times of 17:11 UT (EPAM) and 17:18 UT (EPHIN) support the earlier proton release time based on the first observation of 57.4 MeV protons.

We note that in August 2005 the SOHO spacecraft was oriented so that the ERNE view cones were pointing 45 degrees east of the Sun–Earth line, instead of the nominal 45 degrees west. This attitude may have prevented the observation of the first-arriving field-aligned particles, thus causing a delay in the onset times.

Again, no particle enhancements were observed in the vicinity of the third flare at 14:19 UT on 23 August or during the ascent of the associated very fast halo CME. There was a drop of intensities at middle and high energies late on 23 August related to the ICME, and a small shock peak at lower energies at $\sim 07{:}30 - 09{:}30$ UT on 24 August (Figure 3). There was no indication of a new solar event visible in the electron data at the time of the third flare–CME event, although there was a slight slow increase of near-relativistic electrons starting at $16 - 17$ UT on 23 August.

During the time period of $22 - 23$ August, 2005, the azimuth angle of the IP magnetic field in GSE coordinates was predominantly in the range [90°, 270°] (away from the Sun), although this period occurred in the middle of a negative-polarity sector. During the first and third flare–CME event, the field direction was clearly in this range. At the time of the second event, there were strong fluctuations in the field direction while the field strength remained fairly constant. Nevertheless, during the first and third flare–CME event, the magnetic conditions near Earth were quite similar, and the missing third SEP event cannot be explained by changes in local magnetic conditions.

On the other hand, at the time of the expected third SEP event, the two previous CMEs were still propagating between the Sun and Earth. Because the speed of the second CME was much higher than that of the first (see Table 3), these CMEs were probably merged (see also the discussion in Section 2.3) and could have formed a strong obstacle for the propagation of particles associated with the third flare–CME event.

2.5. Source Regions

2.5.1. 24 November 2000

The three X-class flares on 24 November 2000 were homologous, with a typical two-ribbon structure, and the plasmoid ejections or filament eruptions and CMEs associated with each were observed to have almost the same direction (Takasaki *et al.*, 2004). Several studies on these events have suggested that the flares were triggered by newly emerging flux in the same part of the active region, which led to reconnection and particle acceleration (Nitta and Hudson, 2001; Park *et al.*, 2013). Takasaki *et al.* (2004) also discovered that the rise times of the flares got longer, the plasmoid velocities got smaller, and the separation velocities of the flare ribbons became larger after each event. This may imply that the onsets of the flares occurred in larger flare loops in the later flares and that the reconnection points were higher in the corona.

A detailed study of the second flare–CME event also concluded that several plasmoids were ejected during the flare but were merged into one CME, with the apparent velocity of the CME being higher than those of the plasmoids (Nishizuka *et al.*, 2010). This suggested that the merged plasmoids were continuously accelerated as they were ejected into the IP space.

We compared the large-scale disturbances on the solar disk during each event on 24 November 2000 by analysing the SOHO/EIT difference images. All three events were associated with an EUV wave. Table 4 gives the time of the EIT image when the EUV wave was clearly visible. The partial-view EIT difference images in Figure 4 show the EUV wave front locations with respect to the nominal magnetic footpoint of the Earth. The calculated
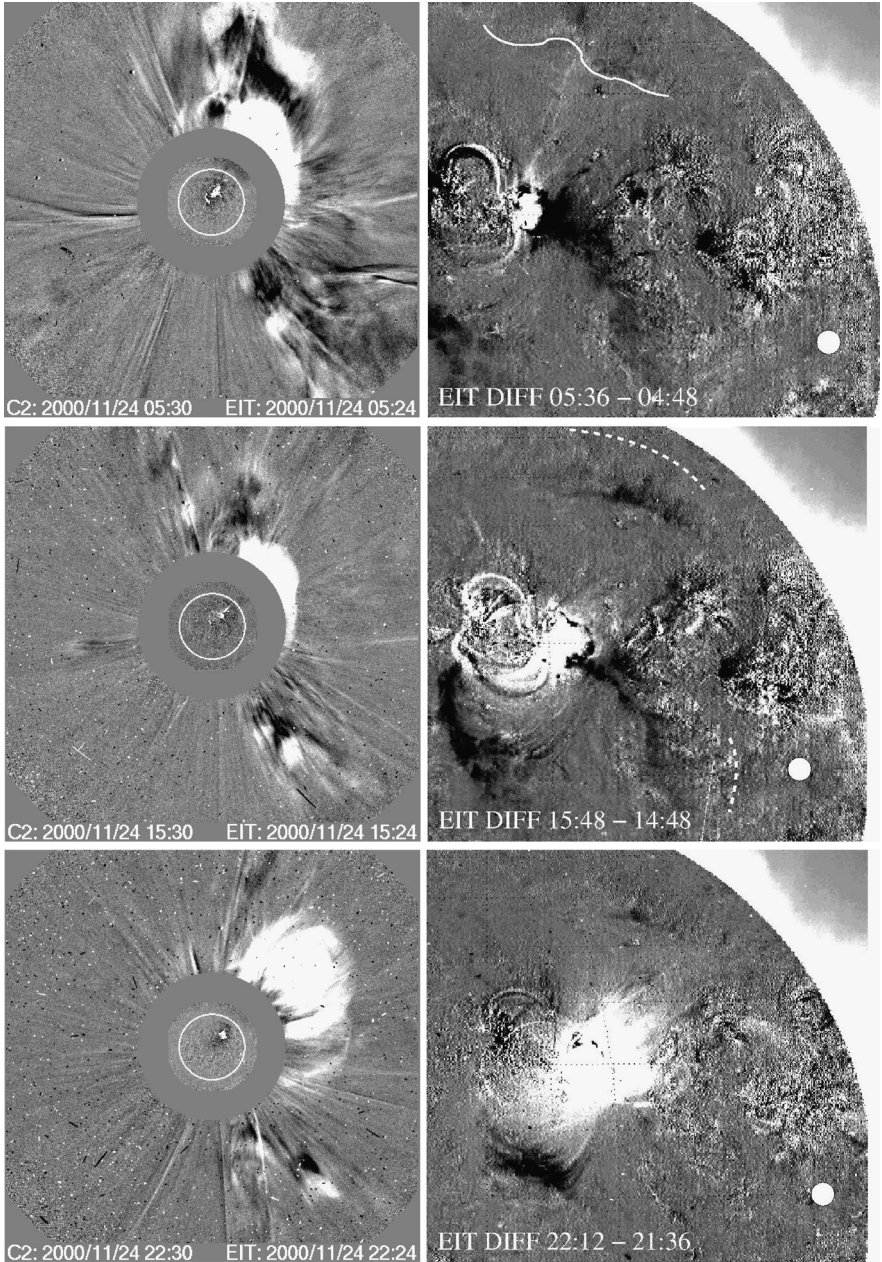
Figure 4 On the left: Difference images showing the coronal mass ejections and the EUV dimming regions near the probable SEP injection times for the three events on 24 November 2000 (SOHO/LASCO C2 and EIT images, from the LASCO CME Catalog). On the right: EIT difference images (195 Å) showing the locations of the EUV waves (marked with white lines, the solid line indicates a clear front and the dashed line a more fuzzy structure). The white filled circle points to the location of the nominal magnetic footpoint of the Earth. The thin black dashed lines in the EIT difference images are the solar grid plotted with 10 degree separation.

footpoint longitudes for the three events were W57–W61, W50–W54, and W56–W60, respectively, with the given range indicating estimated uncertainty resulting from the uncertainty in the used average solar wind speed. The images show that only in the second event the wave appears to reach the magnetic footpoint, and in all events the wave propagation was probably affected by the active regions located in between the burst region and the magnetic footpoint. The third event does not show clear propagating wave fronts.

The only clear qualitative difference between the events was the extent of the dimming regions that appeared after the wave. In the first event two deep separate dimmed regions appeared. In the second event two regions also appeared, but they were spatially smaller. In the third event only one dimmed region appeared. The time separation from flare start to EUV wave detection was 17–21 minutes.

The associated CMEs looked similar at the calculated times of SEP injection (in the first two events when a SEP enhancement was observed) and at the estimated time of SEP injection for the third event (with no SEP enhancement), see Figure 4. Table 4 also gives the estimated height of the CME at the calculated times of SEP injection. In the later CME images there is some indication that the third CME was less sharp-edged at the leading front and less spherical in intensity at larger distances.

2.5.2. 9–11 April 2001

The three flares on 9–11 April 2001 had different X-ray intensities, from M2.3 to X2.3 GOES class. The durations of the first and third flare were similar and much shorter than the second one.

The events on 9–11 April 2001 were also associated with EUV waves (Table 4). The partial-view EIT difference images in Figure 5 show the EUV wave front locations with respect to the nominal magnetic footpoint of the Earth. The calculated footpoint coordinates for the three events were W42–W46, W42–W46, and W34–W38, respectively. In the first and third events the wave appears to reach the magnetic footpoint, but in the second event the wave propagates most noticeably towards the south. In the second event another active region is also located in between the burst region and the magnetic footpoint, which may affect the wave propagation.

As in the 24 November 2000 case, the first two events showed deeper two-part dimmed regions and the dimming in the third was less intense and spatially smaller. The time of the EUV wave listed for the second event in the row (10 April, at 05:24 UT) is later than what is reported in Miteva *et al.* (2014). This is because we list the main wave-like brightening and not the preceding faint transients observed near the erupting active region. The time separation from the flare start to the EUV wave detection was 16–18 minutes.

The appearances of the associated CMEs were again similar. Figure 5 shows the LASCO C2/EIT difference images at the time of the calculated SEP injection time (first event), 0.8 hours after the flare start (second event), and 1.0 hour after the flare start (third event), to show the latter two at the same phase of propagation as the first. The SEP analysis, however, suggests that the SEP injection occurred at a much later time in the second event, about 1.7 hours after the flare start (Table 4).

2.5.3. 22–23 August 2005

The active region that produced the observed flares on 22–23 August 2005 emerged in the middle of a small coronal hole and formed an anemone-like structure (Asai *et al.*, 2009). The region showed a reversed-polarity orientation (in violation of the Hale-Nicholson magnetic
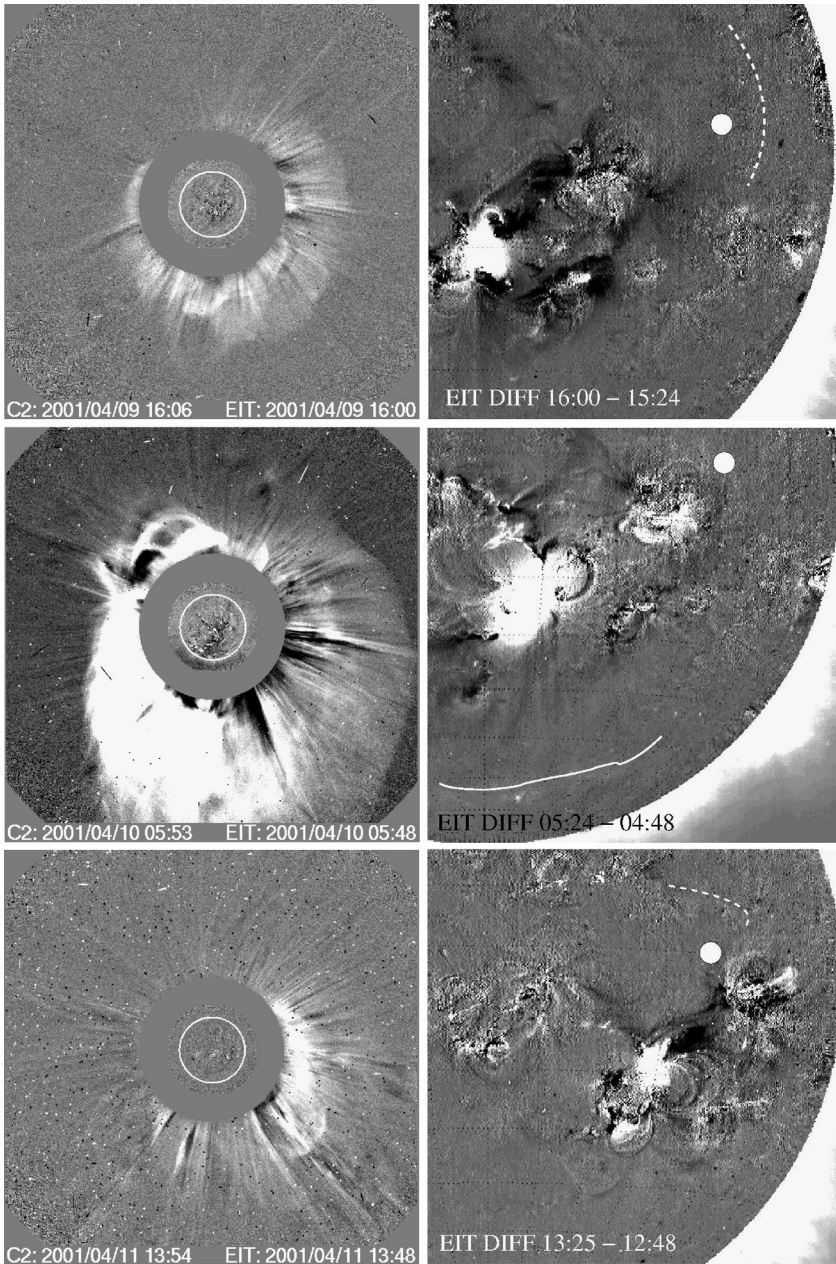
Figure 5 On the left: Difference images showing the coronal mass ejections and the EUV dimming regions near the probable SEP injection times for the three events on 9 – 11 April 2001 (SOHO/LASCO C2 and EIT images, from the LASCO CME Catalog). On the right: EIT difference images (195 Å) showing the locations of the EUV waves (marked with white lines, the solid line indicates a clear front and the dashed line a more fuzzy structure). The white filled circle points to the location of the nominal magnetic footpoint of the Earth. The thin black dashed lines in the EIT difference images are the solar grid plotted with 10 degree separation.

polarity law), which made it statistically more likely to erupt. The magnetic flux and soft X-ray intensity were observed to grow gradually (see Figure 3 in Asai *et al.*, 2009), and the three M-class flares were produced before the active region rotated behind the West limb.

Each event was associated with an EUV wave (Table 4). The partial-view EIT difference images in Figure 6 show the EUV wave front locations with respect to the nominal magnetic footpoint of the Earth. The calculated footpoint coordinates for the three events were W52 – W55, W47 – W51, and W53 – W57, respectively. In the first event the footpoint was basically inside the flaring active region, and in the second and third events, parts of the EUV wave appear to cross the magnetic footpoint region. No obvious qualitative differences were found between the events, although the waves were in general less intense than in the 24 November 2000 and 9 – 10 April 2001 events. The time separation from flare start to the EUV wave detection was 26 – 29 minutes, which is more than in the two other cases.

The associated CMEs were also similar. Figure 6 shows the LASCO C2/EIT difference images near the time of the calculated SEP injection time (first event), 0.7 hours after the flare start (second event), and 0.8 hours after the flare start (third event), to show the latter two at the same phase of propagation as the first. The SEP analysis again suggests that the SEP injection occurred at a much later time in the second event, about 1.6 hours after the flare start (Table 4).

3. Results

We have analysed triple solar events, where intense flares occur in the same active region one after the other (three in a row), each producing an EUV wave, a fast halo-type CME, and a propagating shock wave visible as an interplanetary radio type II burst, and energetic particles associated with at least the first two events. Based on the preliminary event list presented in Table 5 (Appendix) and after using the additional selection criteria described in Section 2, three sequences of events were selected for detailed analyses. These events were observed in the years 2000, 2001, and 2005, and they showed the special feature that while the first two solar bursts were associated with a SEP enhancement, as required, the third was not.

The velocity dispersion analysis (VDA) for the first burst in each sequence gave a solar proton injection time of 0.4 – 0.7 hours after the flare start, at which time the CME was at a height of about 2.5 – 4.0 $R_\odot$. For the second bursts in the row, a delay in the SEP injection time was found in two cases (10 April 2001 and the 22 August 2005 events). A delay in the proton onset times at 1 AU was also reported by Miteva *et al.* (2014). This means that the energetic particles could have been injected some 1.6 – 1.7 hours after the flare, when the CMEs were at heights of about 16.0 – 19.0 $R_\odot$. We note that no delay was observed in the 24 November 2000 case. There the second SEP injection occurred 0.6 hours after the flare start, at which time the CME was at a height of about 3.0 $R_\odot$.

Based on the simple assumption of a 1.2 AU path length, the electron injection times of the first event of the sequences in 2000 and 2001 were consistent with the proton observations. In the sequence of 2005, the agreement was still reasonable, although the derived electron injection times were somewhat earlier than the proton injection time. The agreement was also good in the second event in 2000, while in the two other cases the electron injection seemed to be earlier than proton injection, but still relatively late compared to the flare.

All the nine flare–CME events, in the sequences of three triple events, were associated with large-scale disturbances on the solar disk, observed in EUV. The exact start times of
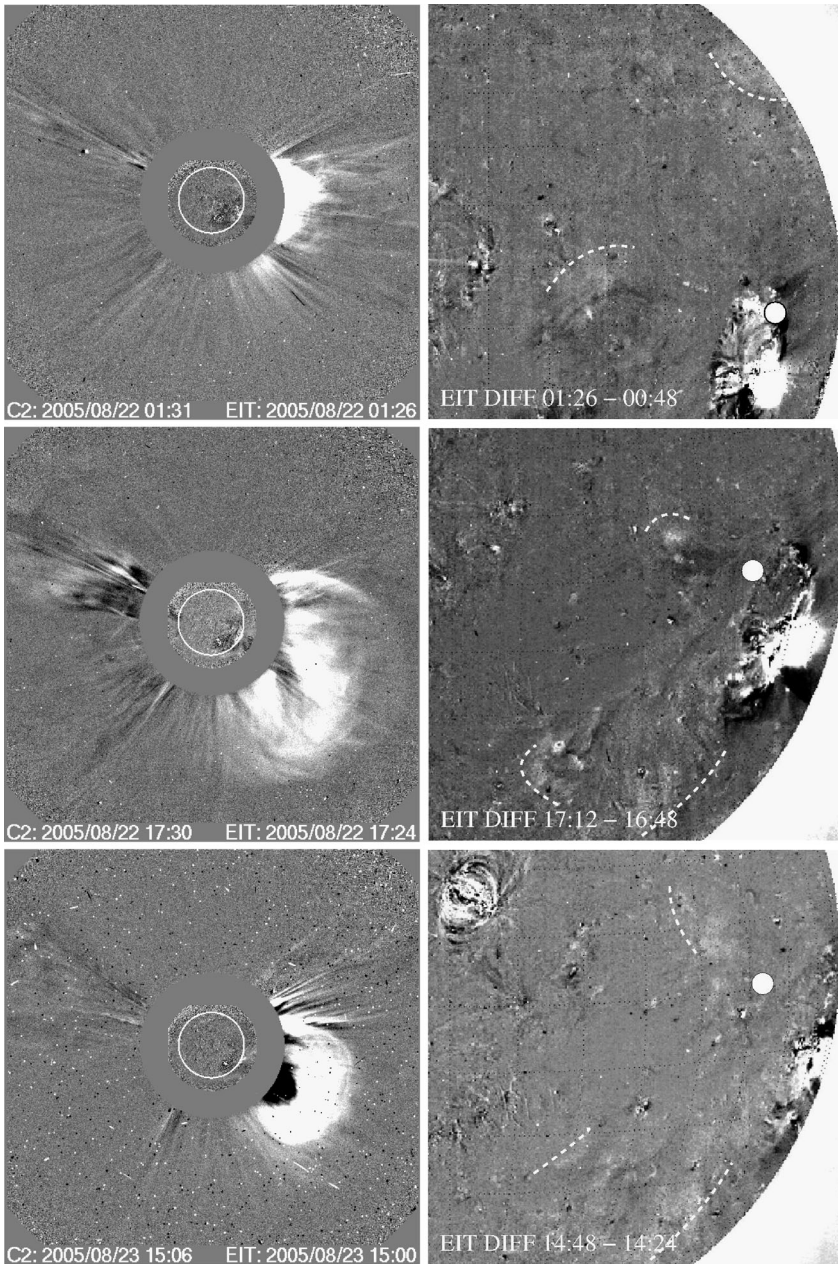
Figure 6 On the left: Difference images showing the coronal mass ejections and the EUV dimming regions near the probable SEP injection times for the three events on 22–23 August 2005 (SOHO/LASCO C2 and EIT images, from the LASCO CME Catalog). On the right: EIT difference images (195 Å) showing the locations of the EUV waves (marked with white lines, the solid line indicates a clear front and the dashed line a more fuzzy structure). The white filled circle points to the location of the nominal magnetic footpoint of the Earth. The thin black dashed lines in the EIT difference images are the solar grid plotted with 10 degree separation.

the EIT (EUV) waves could not be determined because of the low EIT image cadence, but the listed wave observation times (Table 4) show similar timescales in all events. The EUV waves were all followed by dimmings, which typically indicate the depletion of material. We observed that the dimmings in the later events (after the first event in the row) were spatially smaller and less deep, which could mean less ejected material within the CMEs.

All the events were associated with radio type III bursts. However, in each sequence only the first two bursts continued down to the plasma frequency level near Earth, to about 30 kHz. In all three sequences the third type III bursts ended at a higher frequency, near 200 kHz (24 November 2000), 60 kHz (11 April 2001), and 50 – 80 kHz (23 August 2005). These type III cut-off periods lasted for some time, about one day, by which time the associated earlier-launched shocks had arrived at Earth.

Only in April 2001, the inspected *in-situ* magnetic field data indicated a possibility that the magnetic field conditions near Earth would have been such that propagation of particles associated with the third flare–CME event could have been obstructed. These *in-situ* observations, however, do not preclude the possibility that the two previous CME-shock fronts might not have blocked the path of the particles associated with the third flare–CME event for the two other sequences as well.

The first two propagating shocks that started on 24 November 2000 were recorded to arrive near Earth on 26 November. The arrival of the third shock is uncertain, but based on earlier studies, it is possible that the observed shocks (and CMEs) had merged during propagation. The three propagating shocks that started on 9, 10, and 11 April 2001 had corresponding shock arrivals near Earth. The first two CMEs/shocks probably merged to some extent because we note that several shocks were identified at the estimated arrival times of the first two. The third CME on 11 April was identified by IPS measurements, which verifies the height–time evolution. The first two propagating shocks that started on 22 August 2005 were recorded as arriving shocks near Earth on 24 August. Again, merging of the CMEs and shocks appears probable. The arrival near Earth of the third shock, which started on 23 August, was uncertain, but a disturbance was reported to arrive on 25 August, which fits with the estimated height–time evolution.

4. Discussion and Conclusions

We have analysed three sequences of triple flare and CME events originating from the same active region, respectively, on 24 – 26 November 2000, 9 – 13 April 2001, and 22 – 25 August 2005, and their solar energetic particle (SEP) associations. While the propagating shocks in each event could be traced by their interplanetary type II radio emissions, only the first two events in each sequence were associated with SEP enhancements near Earth. The observed radio emission frequencies depend only on the local plasma densities, and the standard atmospheric density models assume spherically symmetric and uniform density structures. However, the actual density structures in the interplanetary medium are both complex and variable (Reiner, 2001). For example, the plasma density corresponding to the frequency of 60 kHz can occur at distances of $45 - 215$ R$_\odot$, depending on the ecliptic longitude (see, for example Figure 9 in Lecacheux *et al.*, 1989). Therefore the obtained type II burst heights can sometimes be questioned, especially at large distances from the Sun. However, shock arrivals near Earth can be registered and compared with the earlier-observed height–time evolution of the propagating shocks. In most of our events shock arrivals were observed.

Since all of the events showed radio type III emission (*i.e.*, fast-drift bursts caused by accelerated electron beams), we investigated their features more closely. Our observation that the type III bursts associated with the third flare–CME events did not reach the near-Earth plasma frequencies deserves attention. It is known that during the propagation of type III radio bursts, the radiation suffers refraction in density gradients and scattering by inhomogeneities (Dulk, 2000). Recent numerical kinetic simulations by Reid and Kontar (2015) have shown that the stopping frequency of type III bursts can be affected by several conditions: the expansion of the guiding magnetic flux tubes, the density and the spectral index of the injected electron beams, and the large-scale density fluctuations in the background electrons. It is very likely that our type III cut-off periods were caused because the Langmuir wave production was stopped, or because the beam paths were diverted before the electron beams reached the Earth. The higher cut-off frequencies could also be explained by higher plasma densities near Earth. However, based on ACE/*Solar Wind Electron, Proton, and Alpha Monitor* (SWEPAM: McComas *et al.*, 1998) solar wind data, there is no indication of an increased plasma density during the 24 November 2000 and 23 August 2005 events. In this respect, the event of 11 April 2001 is different. As the shock arrived at Earth simultaneously with the occurrence of the third flare–CME event of this sequence, there was a sudden increase in the solar wind proton density.

The results from our analyses of the three triple-event sequences suggest that electron beams cannot propagate directly through plasma structures created by at least two earlier CMEs and their associated propagating shocks. The same could be expected for energetic protons. An alternative explanation for not observing SEP enhancement associated with the third flare–CME event would be that the earlier CMEs have wiped out most of the seed particles, with very few particles left for the third CME to accelerate. This possibility is supported by the fact that in the sequences of events in November 2000 and August 2005, no flares were observed between the second and third flare–CME events (from the same active region as the flares of the sequence) and only one C-class flare was reported between the second and third events for the April 2001 sequence. Thus, the seed particle population may have been significantly depleted before the third events of the sequences. In April 2001 there was also a fourth event (without IP type II burst), which was likewise associated with a strong SEP event. However, in this case the event was preceded by three flares (C7.7, B7.2, and M1.3) from the same active region, which could have filled in the seed particle reservoir.

By comparing the flare, EUV wave, CME, and propagating shock wave characteristics, we were unable to find any reason why SEPs would not have been accelerated in all of these events. We suggest that the earlier-launched CMEs and the CME-driven shocks either reduced the seed particle population and thus led to inefficient particle acceleration, or that the propagation paths of both electron beams and SEPs were changed by the effect of the previous eruptions, so that they could not reach the Earth-connected field lines, or that at some point of their propagation between the Sun and Earth they encountered disturbed magnetic fields preventing their propagation to the Earth. For example, during the first two events in each sequence, the geometry of the shock could have been such that it intercepted the interplanetary magnetic field lines connecting to the Earth, while during the third event, particles were injected into magnetic field lines that did not reach the Earth. Hence, particles were not detected near Earth even if the shocks themselves were observed to arrive.

Appendix

The consecutive multiple solar eruptions found from 1997 – 2012 are listed in Table 5.

Table 5 Close-by events that show a flare, a CME, and a decametric-hectometric (DH) type II burst, found from the list of *Wind*/WAVES type II bursts and CMEs at http://cdaw.gsfc.nasa.gov/CME_list/radio/waves_type2.html. The existence of a listed SEP event has been added to each entry (yes). These listed SEP events are taken from Cane, Richardson, and von Rosenvinge (2010) and Richardson *et al.* (2014). The information on the SEP intensities in the non-listed cases are given as rise (flux increasing but not listed as an event), fall (flux decreasing), r/f and f/r (both rise and fall observed, in the given order), flat (constant and unchanging, can be background level or on top of a long-duration event). The observed type III burst cut-offs are also listed in the entries (yes). In this column, $2f_p$ indicates that the bursts end near the second harmonic of the local plasma frequency, AKR stands for auroral kilometric radiation that masks any cut-offs if they exist, and '–' stands for no observed cut-off. The dates with an asterisk indicate the events that are analysed in this article.

Date yyyy/mm/dd	DH type II start (UT)	Start freq. (kHz)	NOAA AR	GOES flare class	CME width (deg)	CME speed fitted $(\mathrm{km\,s}^{-1})$	SEP event	Type III cut-off
1997/11/03	05:15	14000	8100	C8.6	109	227	flat	$2f_p$
1997/11/03	10:30	14000	8100	M4.2	122	352	yes	$2f_p$
1997/11/04	06:00	14000	8100	X2.1	360	785	yes	–
1997/11/06	12:20	14000	8100	X9.4	360	1556	yes	–
2000/11/24*	05:10	14000	9236	X2.0	360	1289	yes	–
2000/11/24*	15:25	14000	9236	X2.3	360	1245	yes	–
2000/11/24*	22:24	4000	9236	X1.8	360	1005	fall	yes
2000/11/25	19:00	6000	9236	X1.9	360	671	rise	yes
2000/11/26	17:00	14000	9236	X4.0	360	980	rise	yes
2001/03/27	02:35	6000	9393	C7.3	60	300	rise	–
2001/03/27	15:00	4000	9393	C5.6	66	340	rise	–
2001/03/29	10:12	4000	9393	X1.7	360	942	yes	–
2001/04/09*	15:53	12000	9415	M7.9	360	1192	yes	–
2001/04/10*	05:24	14000	9415	X2.3	360	2411	yes	–
2001/04/11*	13:15	14000	9415	M2.3	360	1103	fall	yes
2001/04/12	10:20	14000	9415	X2.0	360	1184	yes	–
2002/07/15	21:15	5000	10030	M1.8	> 188	1300	flat	–
2002/07/17	07:30	3500	10030	M8.5	177	716	r/f	–
2002/07/18	07:55	14000	10030	X1.8	360	1099	fall	–
2002/11/09	13:20	14000	10180	M4.6	360	1838	yes	–
2002/11/10	03:20	3000	10180	M2.4	282	1670	r/f	–
2002/11/11	16:15	14000	10180	M1.8	93	1083	fall	$2f_p$

Table 5 (*Continued*)

Date yyyy/mm/dd	DH type II start (UT)	Start freq. (kHz)	NOAA AR	GOES flare class	CME width (deg)	CME speed fitted (km s^{-1})	SEP event	Type III cut-off
2003/05/27	23:12	14000	10365	X1.3	360	964	yes	–
2003/05/28	01:00	1000	10365	X3.6	360	1366	yes	–
2003/05/29	01:10	13000	10365	X1.2	360	1237	flat	–
2004/01/06	00:00	14000	10537	M5.8	166	1469	flat	AKR
2004/01/07	04:15	14000	10537	M4.5	171	1581	flat	AKR
2004/01/07	10:35	14000	10537	M8.3	182	1822	yes	AKR
2004/04/06	13:05	8000	10588	M2.4	360	1368	rise	$2f_p$
2004/04/08	10:25	3000	10588	C7.4	360	1068	rise	–
2004/04/08	13:30	6000	10588	C1.3	92	959	rise	–
2004/11/07	16:25	14000	10696	X2.0	360	1759	yes	–
2004/11/09	17:35	14000	10696	M8.9	360	2000	yes	–
2004/11/10	02:25	14000	10696	X2.5	360	3387	yes	–
2004/12/29	16:35	14000	10715	M2.3	140	774	flat	$2f_p$
2004/12/30	23:45	5000	10715	M4.2	360	1035	flat	$2f_p$
2005/01/01	00:45	14000	10715	X1.7	360	832	flat	–
2005/01/15	06:15	14000	10720	M8.6	360	2049	yes	–
2005/01/15	23:00	3000	10720	X2.6	360	2861	yes	–
2005/01/17	09:25	14000	10720	X2.0	360	2094	yes	–
2005/01/17	09:43	?	10720	X3.8	360	2547	yes	–
2005/01/19	09:20	5300	10720	X1.3	360	2020	fall	–
2005/01/20	07:15	14000	10720	X7.1	360	882	yes	–
2005/08/22*	01:30	8000	10798	M2.6	360	1194	yes	–
2005/08/22*	17:15	12000	10798	M5.6	360	2378	yes	–
2005/08/23*	15:00	13000	10798	M2.7	360	1929	fall	yes
2005/09/09	19:45	10000	10808	X6.2	360	2257	fall	–
2005/09/10	21:45	14000	10808	X2.1	360	1893	flat	$2f_p$
2005/09/11	13:10	3000	10808	M3.0	360	1922	f/r	AKR
2005/09/13	20:20	1100	10808	X1.5	360	1866	yes	–
2011/09/22	11:05	14000	11302	X1.4	360	1905	yes	–
2011/09/24	12:50	16000	11302	M7.1	360	1915	flat	$2f_p$
2011/09/25	05:30	16000	11302	M7.4	193	788	rise	yes
2012/03/07	01:00	16000	11429	X5.4	360	2684	yes	–
2012/03/09	04:10	14000	11429	M6.3	360	950	r/f	yes
2012/03/10	17:55	14000	11429	M8.4	360	1296	flat	$2f_p$
2012/07/05	22:40	3000	11515	M1.6	94	980	yes	–
2012/07/06	23:10	16000	11515	X1.1	360	1828	yes	–
2012/07/08	16:35	16000	11515	M6.9	157	1495	yes	–

References

Al-Sawad, A., Saloniemi, O., Laitinen, T., Kocharov, L.: 2009, *Astron. Astrophys.* **497**, L1. DOI.

Asai, A., Shibata, K., Ishii, T.T., Oka, M., Kataoka, R., Fujiki, K., Gopalswamy, N.: 2009, *J. Geophys. Res.* **114**, A00A21. DOI.

Bougeret, J.-L., Kaiser, M.L., Kellogg, P.J., Manning, R., Goetz, K., Monson, S.J., Monge, N., Friel, L., Meetre, C.A., Perche, C., Sitruk, L., Hoang, S.: 1995, *Space Sci. Rev.* **71**, 231. DOI.

Cane, H.V., Richardson, I.G.: 2003, *J. Geophys. Res.* **108**, 1156. DOI.

Cane, H.V., Richardson, I.G., von Rosenvinge, T.T.: 2010, *J. Geophys. Res.* **115**, A08101. DOI.

Delaboudinière, J.-P., Artzner, G.E., Brunaud, J., Gabriel, A.H., Hochedez, J.F., Millier, F., Song, X.Y., Au, B., Dere, K.P., Howard, R.A., Kreplin, R., Michels, D.J., Moses, J.D., Defise, J.M., Jamar, C., Rochus, P., Chauvineau, J.P., Marioge, J.P., Catura, R.C., Lemen, J.R., Shing, L., Stern, R.A., Gurman, J.B., Neupert, W.M., Maucherat, A., Clette, F., Cugnon, P., van Dessel, E.L.: 1995, *Solar Phys.* **162**, 291. DOI.

Ding, L., Jiang, Y., Zhao, L., Li, G.: 2013, *Astrophys. J.* **763**, 30. DOI.

Dulk, G.A.: 2000. In: Stone, R.G., Weiler, K.W., Goldstein, M.L., Bougeret, J.L. (eds.) *Radio Astronomy at Long Wavelengths*, *AGU Geophys. Monograph Ser.* **119**, 115.

Gold, R.E., Krimigis, S.M., Hawkins, S.E. III, Haggerty, D.K., Lohr, D.A., Fiore, E., Armstrong, T.P., Holland, G., Lanzerotti, L.J.: 1998, *Space Sci. Rev.* **86**, 541. DOI.

Gopalswamy, N.: 2000. In: Stone, R.G., Weiler, K.W., Goldstein, M.L., Bougeret, J.L. (eds.) *Radio Astronomy at Long Wavelengths*, *AGU Geophys. Monograph Ser.* **119**, 123.

Gopalswamy, N., Yashiro, S., Krucker, S., Stenborg, G., Howard, R.A.: 2004, *J. Geophys. Res.* **109**, A12105. DOI.

Iju, T., Tokumaru, M., Fujiki, K.: 2013, *Solar Phys.* **288**, 331. DOI.

Kahler, S.W., Vourlidas, A.: 2005, *J. Geophys. Res.* **110**, A12S01. DOI.

Kahler, S.W., Vourlidas, A.: 2014a, *Astrophys. J.* **784**, 47. DOI.

Kahler, S.W., Vourlidas, A.: 2014b, *Astrophys. J.* **791**, 4. DOI.

Kocharov, L., Laitinen, T., Al-Sawad, A., Saloniemi, O., Valtonen, E., Reiner, M.J.: 2009, *Astrophys. J.* **700**, L51. DOI.

Lecacheux, A., Steinberg, J.-L., Hoang, S., Dulk, G.A.: 1989, *Astron. Astrophys.* **217**, 237.

McComas, D.J., Bame, S.J., Barker, P., Feldman, W.C., Phillips, J.L., Riley, P., Griffee, J.W.: 1998, *Space Sci. Rev.* **86**, 563. DOI.

Miteva, R., Klein, K.-L., Kienreich, I., Temmer, M., Veronig, A., Malandraki, O.E.: 2014, *Solar Phys.* **289**, 2601. DOI.

Müller-Mellin, R., Kunow, H., Fleißner, V., Pehlke, E., Rode, E., Röschmann, N., Scharmberg, C., Sierks, H., Rusznyak, P., McKenna-Lawlor, S., Elendt, I., Sequeiros, J., Meziat, D., Sanchez, S., Medina, J., Del Peral, L., Witte, M., Marsden, R., Henrion, J.: 1995, *Solar Phys.* **162**, 483. DOI.

Nitta, N., Hudson, H.S.: 2001, *Geophys. Res. Lett.* **28**, 3801. DOI.

Nishizuka, N., Takasaki, H., Asai, A., Shibata, K.: 2010, *Astrophys. J.* **711**, 1062. DOI.

Park, S.-H., Kusano, K., Cho, K.-S., Chae, J., Bong, S.-C., Kumar, P., Park, S.-Y., Kim, Y.-H., Park, Y.-D.: 2013, *Astrophys. J.* **778**, 13. DOI.

Papaioannou, A., Mavromichalaki, H., Eroshenko, E., Belov, A., Oleneva, V.: 2009, *Ann. Geophys.* **27**, 1019. DOI.

Pohjolainen, S., Allawi, H., Valtonen, E.: 2013, *Astron. Astrophys.* **558**, A7. DOI.

Pohjolainen, S., van Driel-Gesztelyi, L., Culhane, J.L., Manoharan, P.K., Elliott, H.A.: 2007, *Solar Phys.* **244**, 167. DOI.

Reid, H.A.S., Kontar, E.P.: 2015, *Astron. Astrophys.* **577**, A124. DOI.

Reiner, M.: 2001, *Space Sci. Rev.* **97**, 129. DOI.

Richardson, I.G., von Rosenvinge, T.T., Cane, H.V., Christian, E.R., Cohen, C.M.S., Labrador, A.W., Leske, R.A., Mewaldt, R.A., Wiedenbeck, M.E., Stone, E.C.: 2014, *Solar Phys.* **289**, 3059. DOI.

Smith, C.W., L'Heureux, J., Ness, N.F., Acuña, M.H., Burlaga, L.F., Scheifele, J.: 1998, *Space Sci. Rev.* **86**, 613. DOI.

Takasaki, H., Asai, A., Kiyohara, J., Shimojo, M., Terasawa, T., Takei, Y., Shibata, K.: 2004, *Astrophys. J.* **613**, 592. DOI.

Torsti, J., Valtonen, E., Lumme, M., Peltonen, P., Eronen, T., Louhola, M., Riihonen, E., Schultz, G., Teittinen, M., Ahola, K., Holmlund, C., Kelhä, V., Leppälä, K., Ruuska, P., Strömmer, E.: 1995, *Solar Phys.* **162**, 505. DOI.

Trottet, G., Samwel, S., Klein, K.-L., Dudok de Wit, T., Miteva, R.: 2015, *Solar Phys.* **290**, 819. DOI.

Tylka, A.J., Lee, M.A.: 2006, *Astrophys. J.* **646**, 1319. DOI.

Uwamahoro, J., McKinnell, L.A., Habarulema, J.B.: 2012, *Ann. Geophys.* **30**, 963. DOI.

Vainio, R., Valtonen, E., Heber, B., Malandraki, O.E., Papaioannou, A., Klein, K.-L., Afanasiev, A., *et al.*: 2013, *J. Space Weather Space Clim.* **3**, A12. DOI.

Vršnak, B., Magdalenić, J., Zlobec, P.: 2004, *Astron. Astrophys.* **413**, 753. DOI.

Wang, Y.M., Wang, S., Ye, P.Z.: 2002, *Solar Phys.* **211**, 333. DOI.